9994 *Biochemistry* **2009,** *48,* 9994–10004
DOI: 10.1021/bi901402x

BIOCHEMISTRY
including biophysical chemistry & molecular biology
Article

Chemical and Thermal Unfolding of Glypican-1: Protective Effect of Heparan Sulfate against Heat-Induced Irreversible Aggregation[†]

Gabriel Svensson,*[,‡] Sara Linse,[§] and Katrin Mani*[,‡]

[‡]*Department of Experimental Medical Science, Division of Neuroscience, Glycobiology Group, Lund University, Biomedical Center A13, SE-221 84 Lund, Sweden, and* [§]*Department of Biochemistry, Lund University, Chemical Center, P.O. Box 124, SE-22100 Lund, Sweden*

Received August 12, 2009; Revised Manuscript Received September 23, 2009

ABSTRACT: Glypicans are cell-surface heparan sulfate proteoglycans that influence Wnt, hedgehog, decapentaplegic, and fibroblast growth factor activity via their heparan sulfate chains. However, recent studies have shown that glypican core proteins also have a role in growth factor signaling. Here, we expressed secreted recombinant human glypican-1 in eukaryotic cells. Recombinant glypican-1 was expressed as two glycoforms, one as proteoglycan substituted with heparan sulfate chains and one as the core protein devoid of glycosaminoglycans. Far-UV circular dichroism (CD) analysis of glypican-1 isolated under native conditions showed that the glypican-1 core protein is predominantly α-helical in structure, with identical spectra for the core protein and the proteoglycan form. The conformational stability of glypican-1 core protein to urea and guanidine hydrochloride denaturation was monitored by CD and fluorescence spectroscopy and showed a single unfolding transition at high concentrations of the denaturant (5.8 and 2.6 M, respectively). Renaturation from guanidine hydrochloride gave far-UV CD and fluorescence spectra identical to the spectra of native glypican-1. Thermal denaturation monitored by CD and differential scanning calorimetry (DSC) showed a single structural transition at a temperature of ∼70 °C. Refolding of the heat-denatured glypican-1 core protein was dependent on protein concentration, suggesting that intermolecular interactions are involved in irreversible denaturation. However, refolding was concentration-independent for the proteoglycan form, suggesting that O-glycosylation protects the protein from irreversible aggregation. In summary, we have shown that the glypican-1 core protein is a stable α-helical protein and that the proteoglycan form of glypican-1 is protected from heat-induced aggregation.

Proteoglycans (PGs)[1] are polyanionic macromolecules universally expressed by most cell types. They localize to intracellular granules, are secreted to the extracellular matrix, or are attached to the plasma membrane. PGs consist of a core protein covalently substituted with one or more unbranched polysaccharide chains called glycosaminoglycans (GAGs) (*1*). Glypicans, a family of cell-surface PGs substituted with heparan sulfate (HS) GAG chains, are involved in developmental morphogenesis, growth factor and cytokine signaling, and the uptake of biomolecules, including polyamines, peptides, and nucleic acids, and also viruses (*2*, *3*).

Six glypicans have been identified in vertebrates, two in *Drosophila melanogaster*, one in *Caenorhabditis elegans*, and one in zebrafish (*4*−*6*). The glypican genes have a very characteristic expression pattern during development that reflects important functions for the glypican variants expressed during tissue morphogenesis. Disturbances in glypican gene expression typically result in growth defects and neoplastic transformation, indicating the role in growth factor and morphogen signaling. Many biological functions of glypicans have been related to their HS chains. However, the relative contributions of PG core protein and the HS side chains are an enigma. On the basis of sequence alignments, the glypicans can be divided into two subfamilies. Glypican-1, -2, -4, and -6 have a high degree of homology (40−60%) to each other but are only 20% identical to members of the other group comprising glypican-3 and glypican-5 (which also are 40% identical) (*7*). However, all glypican core proteins are of roughly similar size (60 kDa), and their primary structures have a characteristic pattern involving an N-terminal signal peptide followed by a globular domain containing a unique pattern of 14 conserved Cys residues, a GAG attachment domain restricted to the last 50 amino acids of the C-terminal end that includes multiple Ser-Gly dipeptide sites, and a C-terminal signal peptide responsible for glycosylphosphatidylinositol (GPI) anchorage. The highly conserved features of glypican core proteins suggest that they have important functions, which are now beginning to be understood. Recent studies have revealed a myriad of ligand binding activities of the glypican core proteins. It has been shown that the glypican core proteins bind directly to different growth factors such as hedgehog (*8*, *9*), bone morphogenetic protein 4 (BMP4), decapentaplegic (*10*), and Wnt (*11*)

[†]This work was supported by the Swedish Research Council, the Swedish Cancer Fund, the Medical Faculty of Lund University, the Royal Physiographic Society in Lund, and the Crafoord, Wiberg, Jeansson, Segerfalk, and Kock Foundations.

*To whom correspondence should be addressed. Phone: (46) 46-222 4077. Fax: (46) 46-222 0615. E-mail: katrin.mani@med.lu.se or gabriel.svensson@med.lu.se.

[1]Abbreviations: CD, circular dichroism; DSC, differential scanning calorimetry; FBS, fetal bovine serum; GAG, glycosaminoglycan; Gpc-1, glypican-1; GPI, glycosylphosphatidylinositol; HS, heparan sulfate; MEM, minimal essential medium with Earle's salts; NO, nitric oxide; PG, proteoglycan; SNO, nitrosothiol; T_m, midpoint temperature; TEV, tobacco-etch virus.

 Published on Web 09/23/2009

with significant biological function that is independent of the presence of HS chains, indicating the importance of the core protein structure for the functional activity. A few years ago, Lander and co-workers demonstrated that the HSPG core proteins glypican-1 and -2 and syndecan-3 have ligand-specific influence on protein−PG interactions, by using laminin-1 and FGF-2 as a model system (*12*). Other examples of cell-surface HSPG core proteins that bind to ligands and control their activity in a manner independent of their GAG chains have been documented (*13*), e.g., syndecan-4 to the scaffolding proteins syntenin and CASK (*14*) and syndecan-1 to the catalytic domain of protein kinase Cα (*15*).

We have previously demonstrated that the PG form of glypican-1 (Gpc-1) can be substituted with nitric oxide (NO) and become S-nitrosylated at the Cys residues, forming Gpc-1-SNO (*16*, *17*). The reaction is copper-dependent, and cuproproteins such as the amyloid precursor protein (APP), the prion protein (PrP), and the brain-specific GPI-linked splice variant of ceruloplasmin can deliver Cu(II) ions that are required for S-nitrosylation of Gpc-1 in vitro as well as in vivo (*18*, *19*). Gpc-1-SNO recycles from the cell surface, probably via caveolar endocytosis, to early and late endosomes and then back to the Golgi. In late endosomes, a reducing agent releases NO, which results in deaminative cleavage of the HS chains at N-unsubstituted glucosamines (*20*−*22*). Thus, factors in the Gpc-1 core protein affect the HS chains and modulate their biological function.

The structure and biophysical properties of PGs have been poorly investigated, mainly because of the heterogeneity of the macromolecules. The extracellular matrix PGs decorin and biglycan have been subject to extensive investigations over the past few years. The crystallographic structures of the protein cores of biglycan and decorin were reported recently (*23*, *24*). Cell-surface-bound PGs, glypicans and syndecans, have been more complicated to study because of difficulties in isolating the cell-surface-bound core proteins. In a previous study, we expressed secreted recombinant human Gpc-1 in a eukaryotic system and demonstrated S-nitrosylation of the core protein in the presence of copper(II) ions and NO donor (*17*). To be able to gain insight into the structure of Gpc-1 and its biophysical properties, we have generated recombinant human Gpc-1 (rhGpc-1) lacking the GPI anchor and rhGpc-1 core protein lacking the GPI anchor and the HS attachment sites. When expressed in human embryonic kidney cells, rhGpc-1 lacking the GPI anchor was secreted into the culture medium as both PG and the core protein and rhGpc-1 lacking the GPI anchor and HS attachment sites was secreted solely as the core protein. We have investigated the secondary structure of PG and the core protein using far-UV circular dichroism (CD) spectroscopy. We have also studied the conformational stability of rhGpc-1 core protein and PG using chemical denaturation in urea and guanidine hydrochloride (guanidine-HCl) using CD and fluorescence emission spectroscopy. In addition, the thermostability was investigated by CD spectroscopy and by monitoring the heat capacity using differential scanning calorimetry.

EXPERIMENTAL PROCEDURES

Materials. Plasmid pCEP4-BM40-HisEk, which is derived from the Invitrogen plasmid pCEP4, and human embryonic kidney cells (EBNA 293) were kind gifts from A. Franzén (Lund University). Human Gpc-1 cDNA clone IMAGE ID 6275649 was obtained from Geneservice. All restriction enzymes used were from MBI Fermentas GmbH. Taq polymerase was obtained from Roche. T4 DNA ligase, Lipofectamine, fetal bovine serum (FBS), guanidine-HCl, minimal essential medium with Earle's salts (MEM), 4−12% Bis-Tris SDS−PAGE gels, the colloidal Coomassie blue staining kit, and tobacco-etch virus (TEV) protease were obtained from Invitrogen (Carlsbad, CA). Ni-NTA columns, protein-free medium for CHO cells, and urea were from Sigma-Aldrich (St. Louis, MO). DE-53 diethylaminoethyl was from Whatman. HS lyase (heparitinase) was purchased from Seikagaku Corp.

Plasmid Construction and Mutagenesis. The expression vector used was based on the pCEP4-BM40-HisEk vector described in ref *25*. The enterokinase cleavage site sequence in the pCEP4-BM40-HisEk vector was replaced with a TEV protease site sequence. Two complementary forward and reverse oligonucleotides, 5′-CTGCATCACCATCACCATCACGATCTGTACGAAAACCTGTATTTTCAGGGCA-3′ and 5′-AGCTTGCCCTGAAAATACAGGTTTTCGTACAGATCGTGATGGTGATGGTGATGCAG-3′, respectively, were annealed. The reverse oligonucleotide contained additional bases at the 5′ end to create a *Hin*dIII site. The annealed oligonucleotides were ligated with *Pvu*II/*Hin*dIII-digested pCEP4-BM40-HisEk. The new expression vector was designated pCEP4-BM40-HisTEV. Human Gpc-1 cDNA was amplified by PCR using the forward primer 5′-TT**AAGCTT**GACCCGGCCAGCAAGAG-3′ and the reverse primer 5′-TT**GGATCC**TTAGGTCTTCTGTCCTTCCTGCTC-3′. This created a DNA fragment comprising base pairs 70−1587 of the coding sequence of human Gpc-1 mRNA, as NCBI nucleotide database (GenBank) accession number BC051279. Restriction sites for cloning were inserted at the 5′ end of the primers and are marked in boldface. The PCR product was digested with the restriction enzymes *Bam*HI and *Hin*dIII and inserted into the *Bam*HI/*Hin*dIII-digested pCEP4-BM40-HisTEV plasmid. Mutagenesis was performed using PCR-based site-directed mutagenesis. Gpc-1 cDNA corresponding to base pairs 70−1587 was subcloned into Bluescript vector pKSII. The degenerate forward primer 5′-GACGACGGCAGCGGCACGGGCACCGGTGATGGCTG-3′ and its complement were used to mutate Gpc-1 amino acids 488 and 490 from Ser to Thr. Subsequently, amino acid 486 was mutated from Ser to Thr using the forward primer 5′-CAGGACGCCAGTGACGACGGCACCGGCACG-3′ and its complement. The mutated construct was subcloned back into the expression vector. All constructs were verified by sequencing at Eurofins MWG Operon.

Transfection. Transfection was performed using Invitrogen's standard protocol for transfection with Lipofectamine 2000. The cells were split 1:10 one day after the transfection, and hygromycin B was added to a concentration of 200 μg/mL on the following day. The cells were cloned by limiting dilution after growth for two weeks in the selective medium. Clones expressing a large amount of rhGpc-1 were expanded and used for the study.

Purification of rhGpc-1. Cells expressing rhGpc-1 were grown to confluence in MEM supplemented with 10% (v/v) FBS, 2 mM L-glutamine, penicillin (100 units/mL), streptomycin (100 μg/mL), and 200 μg/mL hygromycin B. After the cells had been extensively washed with PBS, the medium was replaced with protein-free medium supplemented with 2 mM L-glutamine, penicillin (100 units/mL), streptomycin (100 μg/mL), and 100 μg/mL hygromycin B. The conditioned medium was harvested after 3 or 4 days and dialyzed against 0.3 M NaCl and 50 mM sodium phosphate (pH 8.0). The dialyzed conditioned medium was

applied to a Ni-NTA column according to the instructions of the manufacturer. After being extensively washed, the bound rhGpc-1 was eluted in a single peak using a linear imidazole gradient. After removal of the His_6 tag by cleavage with TEV protease, rhGpc-1 was purified further, and the PG form and the core protein were separated by diethylaminoethyl anion-exchange chromatography. Finally, rhGpc-1 was incubated with Ni-NTA resin at 4 °C for 3 h to ensure that all His_6-tagged material had been removed. The purity of the samples was analyzed on a 4−12% Bis-Tris SDS−PAGE gel followed by colloidal Coomassie blue staining. The purified rhGpc-1 core protein was mainly in the monomeric state (>90%), as determined by gel filtration chromatography.

Enzymatic Treatment of rhGpc-1. TEV cleavage was performed in 50 mM Tris-HCl, 0.5 mM EDTA, and 1 mM β-mercaptoethanol (pH 8.0) using 50 units of TEV protease per milligram of rhGpc-1 at 20 °C overnight. HS lyase digestion was performed in 10 mM HEPES, 3 mM $Ca(OAc)_2$, 10 mM EDTA, and 0.1% (v/v) Triton X-100 (pH 7.0) using 2 milliunits of enzyme per 10 μg of rhGpc-1 PG at 37 °C for 2 h.

CD Spectroscopy. Far-UV CD spectra were recorded using a Jasco J-810 spectropolarimeter equipped with a Peltier thermostated cell holder. A 1 mm quartz cuvette was used, and the measurement range was 190−250 nm. The cuvette was thermostated at 20 °C unless otherwise stated. The following parameters were used: sensitivity, 100 mdeg; data pitch, 1 nm; scan rate, 100 nm/min; response time, 4 s; bandwidth, 1 nm; and accumulation, 2. Baseline spectra were recorded for pure buffer and subtracted from the corresponding protein spectra. A stock solution of rhGpc-1 was clarified by centrifugation at 15000*g* for 15 min, and the protein concentration was determined using the bicinchoninic acid protein assay (Pierce Biotechnology, Rockford, IL). Bovine serum albumin was used as a protein standard. Samples were prepared by dilution of the rhGpc-1 stock solution to 0.1 mg/mL in 20 mM sodium phosphate (pH 7.4) or in urea or guanidine-HCl in 20 mM sodium phosphate (pH 7.4). High-purity urea and guanidine-HCl were used in these experiments. Samples with denaturant were incubated overnight at room temperature before CD spectra were recorded. The secondary structure fractions of rhGpc-1 core protein were estimated by deconvolution of the CD spectra using CDPro (*26*). Mean residue ellipticity was calculated using 110.5 as the mean residue molecular weight of Gpc-1. CD spectra were recorded for rhGpc-1 from several different preparations.

Fluorescence Spectroscopy. Fluorescence spectra were recorded using a Jasco J-810 spectropolarimeter. A 2 mm × 10 mm quartz cuvette was used. The excitation wavelength was 280 nm, and emission was recorded between 310 and 400 nm. The following parameters were used: sensitivity, 700 V; data pitch, 1 nm; response time, 0.5 s; bandwidth, 5 nm; and accumulation, 2. The cuvette was thermostated at 20 °C. The protein concentration was 30 μg/mL in 20 mM sodium phosphate (pH 7.4).

Chemical Denaturation and Data Analysis. Urea and guanidine-HCl denaturation curves were obtained by monitoring the CD and fluorescence of 0.1 mg/mL rhGpc-1 in different concentrations of urea or guanidine-HCl. Solutions with 35 different concentrations of urea ranging from 0 to 8.55 M were prepared by diluting a stock solution of 10 M urea and 20 mM sodium phosphate (pH 7.0) with 20 mM sodium phosphate (pH 7.0). The pH of the different preparations was adjusted, and the protein was diluted to 0.1 mg/mL from a stock solution. Samples with 25 different guanidine-HCl concentrations ranging from 0 to 6.09 M were prepared by mixing two stock solutions with 1.4 μM rhGpc-1 and either 7 M guanidine-HCl or 0 M guanidine-HCl, in 100 mM sodium phosphate (pH 8.0). These samples were allowed to equilibrate overnight at room temperature, after which the CD signal was measured at 222 nm for 1 min (the data obtained were averaged) and the fluorescence intensity measured at 320 nm with an excitation wavelength of 280 nm. The sensitivity was 600 V for the fluorescence measurements. CD was measured in a 2 mm path length quartz cuvette, and fluorescence was measured in a 2 mm × 10 mm cuvette.

The data from the urea and guanidine-HCl denaturation curves were analyzed using a linear extrapolation method assuming reversible two-state unfolding (*27*, *28*). Y_o is the observed ellipticity or fluorescence intensity at a given denaturant concentration.

$$Y_0 = Y_N/(1+K_{NU}) + Y_U K_{NU}/(1+K_{NU}) \quad (1)$$

where Y_N is the signal from the native form, Y_U is the signal from the denatured form, and K_{NU} is the equilibrium constant.

$$K_{NU} = [U]/[N] \quad (2)$$

The denaturant-dependent signals from native and denatured states were treated as straight lines

$$Y_N = k_N[D] + b_N \quad (3)$$

$$Y_U = k_U[D] + b_U \quad (4)$$

where k_N and k_U are the slopes, b_N and b_U are the intercepts, and [D] is the denaturant concentration.

The free energy of the unfolding was assumed to vary linearly with denaturant concentration

$$\Delta G_{NU} = \Delta G_{NU}(H_2O) - m_D[D] \quad (5)$$

where $\Delta G_{NU}(H_2O)$ is the free energy change in the absence of denaturant and m_D is the slope. The equilibrium constant as a function of denaturant is

$$K_{NU} = e^{-(\Delta G_{NU}(H_2O) - m_D[D])} \quad (6)$$

Incorporating eqs 2−6 into eq 1 yields the following equation:

$$Y_0 = \{(k_N[D] + b_N) + (k_U[D] + b_U)e^{-[\Delta G_{NU}(H2O) - m_D[D]]/RT}\} / \{1 + e^{-[\Delta G_{NU}(H2O) - m_D[D])/RT}\} \quad (7)$$

which was fitted to the data. R is the molar gas constant, and T is the temperature. Kaleidagraph (Synergy Software) was used to fit the data using nonlinear least-squares analysis. After being fit, the data were normalized to F_{app}, the apparent fraction unfolded, using the equation

$$F_{app} = (Y_0 - Y_N)/(Y_U - Y_N) \quad (8)$$

Heat Denaturation and Data Analysis. Heat denaturation was studied using CD spectroscopy. rhGpc-1 (0.1 mg/mL) in 20 mM sodium phosphate (pH 7.4) was heated from 20 to 90 °C at a rate of 1 °C/min. The following parameters were used: wavelength, 208 nm; sensitivity, 100 mdeg; data pitch, 1 °C; delay time, 1 min; response, 4 s; bandwidth, 1 nm.

Differential scanning calorimetry was performed using a VP-DSC microcalorimeter from Microcal (Northampton, MA). His-tagged rhGpc-1 was dialyzed extensively against 20 mM sodium phosphate (pH 7.4). The protein solution was clarified by centrifugation, and the protein concentration (0.1−1 mg/mL)

was determined using the bicinchoninic acid protein assay. Buffer and protein solutions were degassed under mild vacuum prior to the experiment. The solution was heated from 10 to 90 °C at a rate of 1 °C/min. An excess pressure of 1.7 atm was applied to the cells during the experiments. After the microcalorimeter cells had been cooled to 10 °C and after a 15 min prescan thermostat at 10 °C, a second scan from 10 to 90 °C was performed to study whether the protein had refolded.

The calorimetric data were analyzed using Origin (version 7.0383) provided by Microcal. The analyses were based on the equation

$$C_p = C_{p\mathrm{N}} + \left[\frac{K_\mathrm{A}\Delta C_{p\mathrm{A}}}{1+K_\mathrm{a}} + \frac{K_\mathrm{A}\Delta H_\mathrm{A}^*\Delta H_\mathrm{A}}{(1+K_\mathrm{A})^2 RT^2}\right] \quad (9)$$

where C_p is the total molar heat capacity, $C_{p\mathrm{N}}$ is the molar heat capacity of the totally folded state, $\Delta C_{p\mathrm{A}}$ is the change in heat capacity for unfolding of a structural domain A, K_A is the corresponding equilibrium constant, ΔH_A^* is the van't Hoff heat change (the heat change for the cooperative unit that participates in the reaction), ΔH_A is the heat change, R is the molar gas constant, and T is the temperature.

Two models were used. The first was a two-state model based on the equations

$$C_p(T) = \frac{K_\mathrm{A}(T)\Delta H_\mathrm{A}(T)^2}{[1+K_\mathrm{A}(T)]^2 RT^2} \quad (10)$$

$$K_\mathrm{A}(T) = \mathrm{e}^{\left[\frac{-\Delta H_{\mathrm{mA}}}{RT}\left(1-\frac{T}{T_{\mathrm{mA}}}\right)\right]} \quad (11)$$

Before the data were fit, a progress baseline was subtracted from the calorimetric data, thus treating ΔC_p as zero. $C_{p\mathrm{N}}$ is therefore equal to zero at all temperatures, and ΔH_A is temperature-independent (ΔH_{mA}). Since the model assumes that the transition is a two-state transition, the van't Hoff ΔH^* values are equal to the calorimetric heat change ΔH_A. The fitting parameters were T_{mA} and ΔH_{mA}, and the equations were fitted to the experimental data using nonlinear least-squares.

The second model was a non-two-state model, also treating ΔC_p as zero. Since this is a non-two-state model, it includes the van't Hoff heat change according to

$$C_p(T) = \frac{K_\mathrm{A}(T)\Delta H_{\mathrm{mA}}^*\Delta H_{\mathrm{mA}}}{[1+K_\mathrm{A}(T)]^2 RT^2} \quad (12)$$

$$K_\mathrm{A}(T) = \mathrm{e}^{\left[\frac{-\Delta H_{\mathrm{mA}}^*}{RT}\left(1-\frac{T}{T_{\mathrm{mA}}}\right)\right]} \quad (13)$$

The fitting parameters were T_{mA}, ΔH_{mA}, and ΔH_{mA}^*, and the equations were fitted to the experimental data using nonlinear least-squares.

The Gibbs free energy change at 20 °C [ΔG (*20*)] was calculated using the equation

$$\frac{\Delta G}{T} = \Delta H(T_\mathrm{m})\left(\frac{1}{T}-\frac{1}{T_\mathrm{m}}\right) + \Delta C_p\left(\ln\frac{T_\mathrm{m}}{T} - \frac{T_\mathrm{m}}{T} + 1\right) \quad (14)$$

where T_m is the temperature midpoint, $\Delta H(T_\mathrm{m})$ is the enthalpy change at T_m, and ΔC_p is the change in heat capacity at T_m.

Buffer−buffer scan reference data were subtracted from all DSC profiles presented. Refolding was calculated by comparing the area under the DSC curve after baseline subtraction for the first and second scans.

Scheme 1: Structure of Human Gpc-1 Compared to the rhGpc-1 Used in This Study[a]

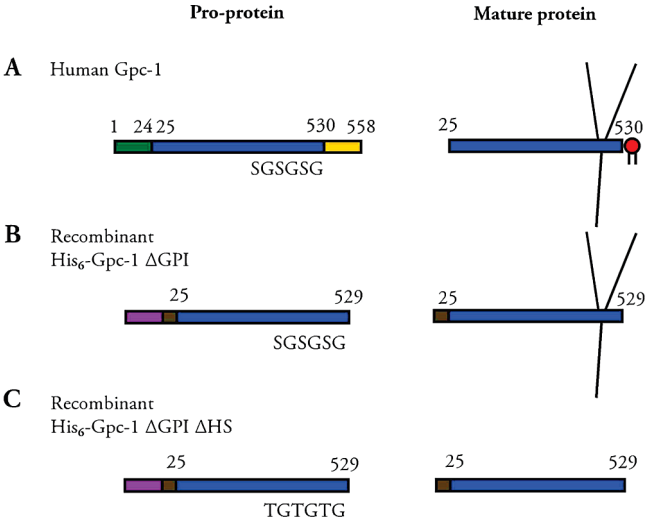

[a](A) The human Gpc-1 pro-protein consists of N- and C-terminal signal peptides (green and yellow bars, respectively) and core protein (blue bar). Gpc-1 also contains attachment sites for N-linked glycosylation (not shown) and O-linked glycosylation (indicated as clustered SG sequences). The mature proteoglycan contains N-linked glycans (not shown) and O-linked glycans at Ser 486, 488, and 490 (thin solid lines) and is GPI-anchored at Ser 530 (red circle with two lines). (B) In recombinant His_6-Gpc-1 ΔGPI, the two signal peptides were replaced with an N-terminal BM40 secretion peptide (purple bar), a His_6 tag, and a TEV protease cleavage site (brown bar). (C) In His_6-Gpc-1 ΔGPI ΔHS, the Ser residues in the attachment sites for O-linked glycosylation were replaced with Thr residues (indicated as TGTGTG). The numerals in the scheme indicate amino acids in Gpc-1. The images are not drawn to scale.

RESULTS

Gpc-1 Expression Vectors. Two expression vectors were created for production and secretion of rhGpc-1 in human embryonic kidney cells. The first vector was made via introduction of a cDNA (GenBank accession number BC051279) encoding the mature Gpc-1 core protein into the pCEP4-BM40-HisTEV vector. The sequence encoding the Gpc-1 N-terminal signal peptide responsible for translocation to the ER was not introduced into the vector. Also omitted was the C-terminal signal peptide responsible for attachment of GPI to the membrane. The vector thus encoded a BM40 secretion peptide, a His_6 tag, and a TEV protease cleavage site followed by the mature form of the Gpc-1 core protein. In what follows, this vector will be termed pGpc-1 ΔGPI. pGpc-1 ΔGPI was further developed to create another vector, encoding the Gpc-1 core protein devoid of O-linked glycosylation. The sequence encoding the HS attachment sites in Gpc-1 was mutated to encode Thr instead of Ser at positions 486, 488, and 490. This vector will be termed pGpc-1 ΔGPI ΔHS. The structures of Gpc-1 and of the rhGpc-1 encoded by the vectors are compared in Scheme 1.

Expression and Purification of rhGpc-1. Human embryonic kidney cells were transfected with the pGpc-1 ΔGPI vector. After growth in selective medium for 2 weeks, the cells were cloned by limiting dilution. Cell clones were grown to confluence and were then maintained in protein-free medium, which was harvested after 3 or 4 days. The conditioned medium was analyzed via SDS−PAGE with a gel stained with Coomassie blue (data not shown). Clones with a high level of expression of putative rhGpc-1 were selected and used in further studies.

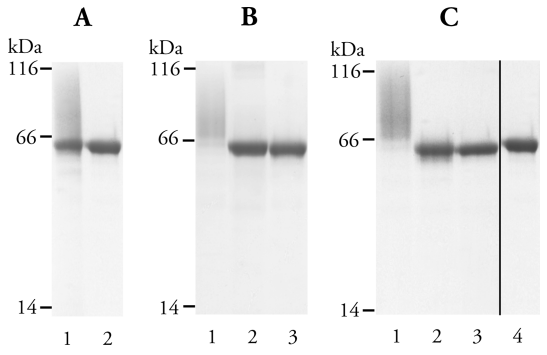

FIGURE 1: SDS−PAGE analysis of rhGpc-1. (A) SDS−PAGE and Coomassie blue staining of Ni-NTA-purified rhGpc-1 from pGpc-1 ΔGPI-transfected cells (lane 1) and from pGpc-1 ΔGPI ΔHS-transfected cells (lane 2). (B) Gpc-1 PG and the core protein expressed by pGpc-1 ΔGPI-transfected cells were separated by anion-exchange chromatography. The PG (lane 1) and the HS lyase-digested PG (lane 2) were subjected to SDS−PAGE and Coomassie blue staining. The control core protein band is shown in lane 3. (C) SDS−PAGE and Coomassie blue staining of different rhGpc-1 proteins after removal of the His_6 tag using TEV protease: Gpc-1 ΔGPI PG (lane 1), Gpc-1 ΔGPI core protein (lane 2), and Gpc-1 ΔGPI ΔHS (lane 3). His_6-Gpc-1 ΔGPI ΔHS was used as a control (lane 4). To each well was added 2 μg of purified protein.

A large batch of conditioned medium (~150 mL) was harvested and applied to a Ni-NTA column. A single peak of protein was eluted from the column using a linear imidazole gradient. The protein was analyzed via SDS−PAGE with a gel stained with colloidal Coomassie blue and yielded a band with an M_r of ~65 kDa and a smear with an M_r of ~65−120 kDa (Figure 1A, lane 1). MALDI-TOF experiments identified what appeared to be the rhGpc-1 core protein at an M_r of ~65 kDa as Gpc-1 with a sequence coverage of 37% (data not shown). Both the rhGpc-1 core protein band and the putative PG smear reacted with an antibody to Gpc-1 using Western blotting (data not shown). The putative rhGpc-1 PG was separated from the core protein by anion-exchange chromatography and visualized via SDS−PAGE with a gel stained with Coomassie blue before and after enzymatic degradation with HS lyase (Figure 1B, lanes 1 and 2). As shown, digestion with HS lyase yielded a band of ~65 kDa corresponding to the Gpc-1 core protein, indicating degradation of the HS side chains. Thus, we had expression of both rhGpc-1 core protein and PG. Similar results have been obtained by overexpressing the PG decorin, which also becomes expressed both as a core protein and as PG (*29*). In what follows, the rhGpc-1 expressed by the pGpc-1 ΔGPI vector is termed His_6-Gpc-1 ΔGPI core protein and His_6-Gpc-1 ΔGPI PG. Human embryonic kidney cells were also transfected with pGpc-1 ΔGPI ΔHS. The cells were cloned and analyzed as described for the cells transfected with pGpc-1 ΔGPI. Protein purified from conditioned medium appeared as a single band without a PG smear (Figure 1A, lane 2), indicating that no HS was added to the core protein. Interestingly, the mutation of the HS attachment sites in Gpc-1 resulted in a 10-fold increase in the level of protein expression, with yields of up to 10 mg/100 mL of conditioned medium. This rhGpc-1 will be termed His_6-Gpc-1 ΔGPI ΔHS. The His_6 tag was removed from His_6-Gpc-1 ΔGPI PG, His_6-Gpc-1 ΔGPI core protein, and His_6-Gpc-1 ΔGPI ΔHS by cleavage with TEV protease, and it was further purified as indicated in Experimental Procedures. No unspecific cleavage was seen upon cleavage with TEV protease (Figure 1C). The three forms of rhGpc-1 in which the His_6 tag has been removed will be termed Gpc-1 ΔGPI PG (Figure 1C, lane 1), Gpc-1 ΔGPI core protein (Figure 1C, lane 2), and Gpc-1 ΔGPI ΔHS (Figure 1C, lane 3).

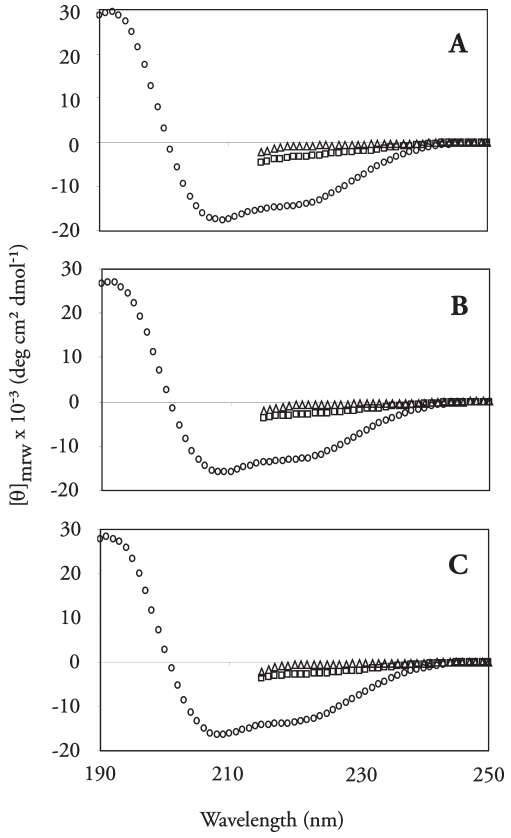

FIGURE 2: Far-UV CD spectra of native and chemically denatured rhGpc-1. Far-UV CD spectra of (A) Gpc-1 ΔGPI PG, (B) Gpc-1 ΔGPI core protein, and (C) Gpc-1 ΔGPI ΔHS in 20 mM sodium phosphate (pH 7.4) (○), 8 M urea (□), or 6 M guanidine-HCl (△). Samples with denaturant were incubated overnight at room temperature before the CD spectra were recorded. All spectra were measured at 20 °C.

Far-UV CD and Fluorescence Spectra of Native and Denatured rhGpc-1. The far-UV CD spectra of Gpc-1 ΔGPI PG, Gpc-1 ΔGPI core protein, and Gpc-1 ΔGPI ΔHS were recorded under native and denaturing conditions. The spectrum of Gpc-1 ΔGPI PG in 20 mM sodium phosphate (pH 7.4) exhibited a peak at 195 nm and two troughs at 208 and 222 nm, which is characteristic of a protein containing α-helices (Figure 2A). The spectrum was compared to those of a reference set of 43 different proteins using the CDPro software package (*26*). By this analysis, the secondary fractions in Gpc-1 ΔGPI PG were estimated to be around 42% in α-helical structure, 13% in β-sheet conformation, 18% in turns, and 27% unordered. The spectra of the Gpc-1 ΔGPI core protein and Gpc-1 ΔGPI ΔHS in 20 mM sodium phosphate were identical to the Gpc-1 ΔGPI PG spectrum [Figure 2A−C (○)]. An almost complete disappearance of the CD signal was observed for all three rhGpc-1 forms after incubation in 8 M urea and 6 M guanidine-HCl overnight [Figure 2A−C (□ and △, respectively)], indicating loss of all secondary structure at high concentrations of chaotropes. The spectral identity between the three forms of rhGpc-1 implies that neither the presence of HS chains nor the mutations in Gpc-1 ΔGPI ΔHS affect the secondary structure.

Gpc-1 contains six Trp and 11 Tyr residues, which made it possible to study the conformation of Gpc-1 using fluorescence

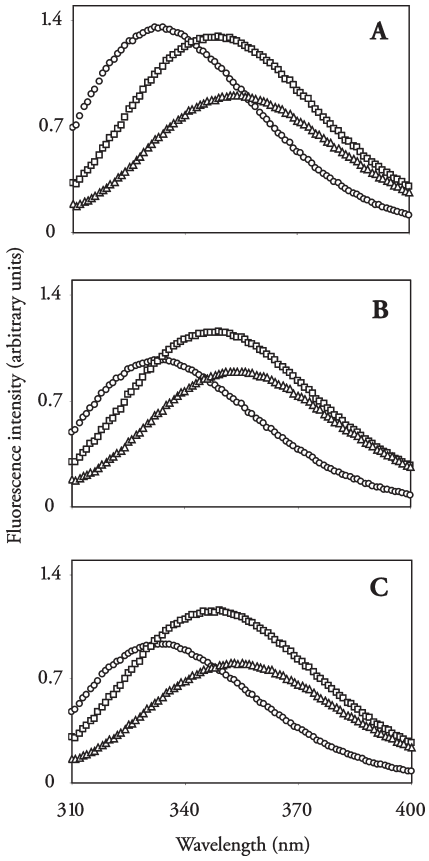

FIGURE 3: Fluorescence emission spectra of native and chemically denatured rhGpc-1. Fluorescence spectra of (A) Gpc-1 ΔGPI PG, (B) Gpc-1 ΔGPI core protein, and (C) Gpc-1 ΔGPI ΔHS in 20 mM sodium phosphate (pH 7.4) (○), 8 M urea (□), or 6 M guanidine-HCl (△). The excitation wavelength was 280 nm. Samples with denaturant were incubated overnight at room temperature before the CD spectra were recorded. All spectra were measured at 20 °C.

emission spectroscopy. Trp-290 and Trp-416 are evolutionarily conserved in all human glypicans, while Trp-167 and Trp-393 are conserved in glypican-1, -2, -4, and -6. The Trp → Arg mutation in glypican-3 of the amino acid corresponding to Trp-290 in Gpc-1 has been found in a Simpson-Golabi-Behmel syndrome patient, and it results in poor addition of HS chains (*7*). Tyr-424 is the only Tyr residue that is evolutionarily conserved in all glypicans. However, many of the other Tyr residues share homology between three or four of the glypicans. Together, this suggests that the Trp and Tyr residues are important for stabilizing the conformation of glypicans. The fluorescence emission spectra of rhGpc-1 were recorded in 20 mM sodium phosphate (pH 7.4) (excitation wavelength of 280 nm, exciting both Trp and Tyr). For all three forms of rhGpc-1, the fluorescence emission maximum was 333 nm [Figure 3A−C (○)]. This is consistent with fluorescence emission maxima of natively folded proteins, which are usually between 330 and 340 nm. Denaturation in 8 M urea overnight shifted λ_{max} to 349 nm [Figure 3A−C (□)]. λ_{max} is dependent on the polarity of the immediate environment around the Trp residues, and a shift toward 350 nm indicates that the Trp residues are fully exposed to solvent. Thus, the λ_{max} at 349 nm for rhGpc-1, which had been exposed to 8 M urea overnight, indicates that denaturation leads to full exposure of the tryptophan side chains to water. Full exposure was also observed with rhGpc-1, which had been exposed to 6 M guanidine-HCl, with λ_{max} at 354 nm [Figure 3A−C (△)]. The fluorescence emission data confirmed the far-UV CD data, giving the same results for all three forms of rhGpc-1. The differences seen in fluorescence intensities could have many causes, and they are more difficult to interpret than the shifts in λ_{max}.

Stability and Refolding of His$_6$-Gpc-1 ΔGPI ΔHS. The conformational stability of rhGpc-1 with respect to urea and guandine-HCl denaturation was investigated with His$_6$-Gpc-1 ΔGPI ΔHS. On the basis of the CD and fluorescence spectra shown in Figures 2 and 3, we measured the ellipticity at 222 nm and the fluorescence at 320 nm (excitation at 280 nm) of His$_6$-Gpc-1 ΔGPI ΔHS, which had been incubated overnight in 0−8.55 M urea or 0−6.09 M guanidine-HCl. It is evident from these data that rhGpc-1 is a stable protein that resists denaturation up to high concentrations of urea or guanidine-HCl. Moreover, the steepness of the transition zone data indicates a highly cooperative unfolding process. All data were well fitted using a two-state model (native protein in equilibrium with unfolded protein) assuming a linear dependence of the free energy of unfolding on the denaturant concentration (Figure 4). Fitting to CD and fluorescence data using eq 7 (see Experimental Procedures) yielded close to identical values of $\Delta G^\circ_{H_2O}$ and m, for data both in urea and in guanidine-HCl. The transition occurred at the same concentrations for both the secondary structure as monitored by CD spectroscopy and the tertiary structure as monitored by fluorescence spectroscopy. This is a strong indication that CD and fluorescence report on the same process and that the unfolding equilibrium is a two-state process with no intermediates. Fitting to urea denaturation data by CD yields a $\Delta G^\circ_{H_2O}$ of 59.2 kJ/mol and an m of 10.1 kJ L mol^{-2} and by fluorescence gives a $\Delta G^\circ_{H_2O}$ of 59.1 kJ/mol and an m of 10.2 kJ L mol^{-2} (Figure 4A,B). From these values, the urea concentration at 50% unfolding was calculated to be $C_M = \Delta G^\circ_{H_2O}/m$ = 5.8 M. Also for guanidine-HCl, the transition from folded to unfolded occurred at the same concentrations for the secondary and tertiary structures. Fitting to guanidine-HCl data by CD yields a $\Delta G^\circ_{H_2O}$ of 64.2 kJ/mol and an m of 24.4 kJ L mol^{-2} and by fluorescence gives a $\Delta G^\circ_{H_2O}$ of 63.9 kJ/mol and an m of 24.5 kJ L mol^{-2} (Figure 4C,D). From these values, the guanidine-HCl concentration at 50% unfolding was calculated to be $C_M = \Delta G^\circ_{H_2O}/m$ = 2.6 M. The baseline values obtained by fitting eq 7 to the raw data were used to normalize the data, resulting in the graphs shown in panels E and F of Figure 4. The very close correspondence between data obtained by CD and fluorescence is evident from these normalized data, both for urea and for guanidine-HCl denaturation.

Fitting to urea and guanidine-HCl data gave a small difference in the extrapolated stability in the absence of denaturant ($\Delta G^\circ_{H_2O}$ = 59 and 64 kJ/mol, respectively). This could be due to the uncertainty of using very long extrapolations or to the fact that extrapolation is from quite different solution conditions in terms of electrostatic shielding. The guanidine-HCl denaturation curve was obtained in the presence of 0.1 M sodium phosphate to partly compensate for the very large differences in ionic strength between low and high concentrations of guanidine-HCl.

We also investigated whether it was possible to refold His$_6$-Gpc-1 ΔGPI ΔHS after denaturing the protein in 6.4 M guandine-HCl overnight at room temperature. We first confirmed by CD and fluorescence spectroscopy that His$_6$-Gpc-1 ΔGPI ΔHS was denatured and then dialyzed the sample against 20 mM sodium phosphate (pH 7.4). The far-UV CD and fluorescence spectra of renatured His$_6$-Gpc-1 ΔGPI ΔHS were identical to the spectra of native His$_6$-Gpc-1 ΔGPI ΔHS (data not

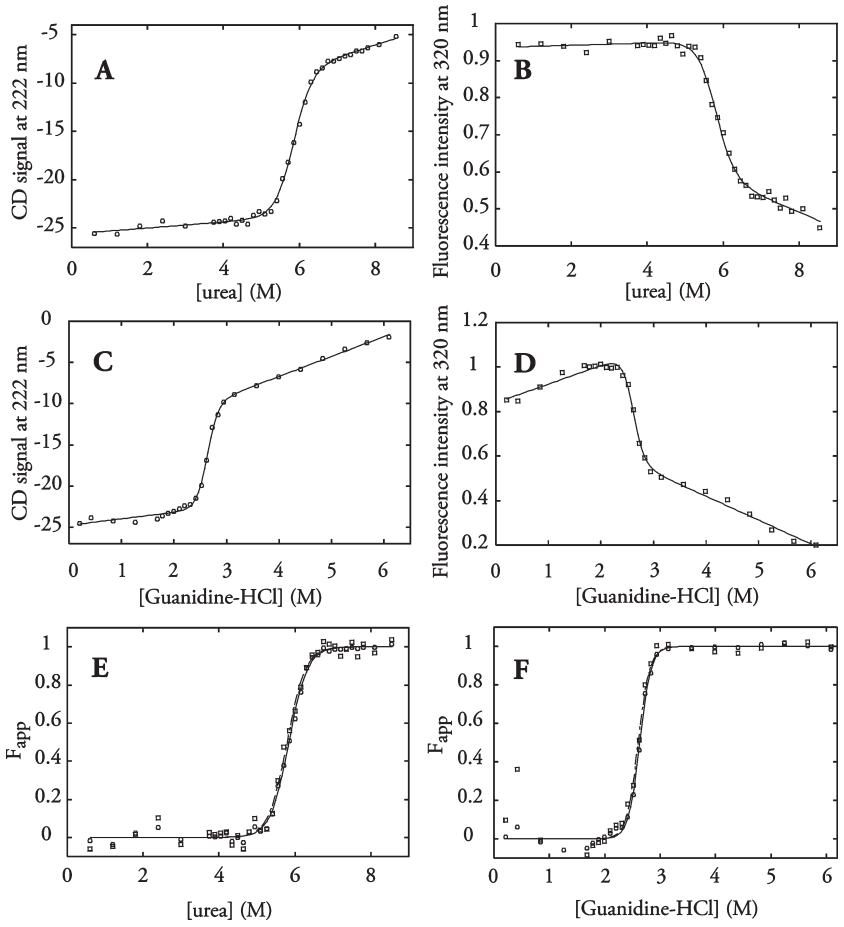

FIGURE 4: Denaturation of His_6-Gpc-1 ΔGPI ΔHS by urea or guandine-HCl monitored by far-UV CD and fluorescence. His_6-Gpc-1 ΔGPI ΔHS was incubated overnight in increasing concentrations of urea (A and B) or guanidine-HCl (C and D). Unfolding was monitored by ellipticity at 222 nm (○, A and C) or fluorescence at 320 nm (□, B and D). The CD and fluorescence data were fitted using a two-state model (—). (E and F) Data for the urea and guanidine-HCl denaturation were normalized to apparent fraction unfolded (F_{app}): (○) normalized CD, (□) normalized fluorescence, (—) fitted curve CD, and (– – –) fitted curve fluorescence.

shown). However, the signal intensity was reduced by approximately one-third, indicating that a substantial proportion of the material was lost after exchange of guanidine-HCl back to sodium phosphate.

Heat Denaturation of rhGpc-1. The thermal stability of rhGpc-1 was investigated using CD spectroscopy. Gpc-1 ΔGPI PG, Gpc-1 ΔGPI core protein, and Gpc-1 ΔGPI ΔHS in 20 mM sodium phosphate (pH 7.4) were heated at a rate of 1 °C/min, and the ellipticity at 208 nm was monitored. A sharp decrease in the signal obtained occurred at ~70 °C for both the Gpc-1 ΔGPI core protein and Gpc-1 ΔGPI ΔHS (Figure 5A). This indicates considerable stability to thermal unfolding and that the temperature at the transition midpoint is around 70 °C. Unfolding of Gpc-1 ΔGPI PG took place at a lower temperature (~65 °C) with a greater reduction in the magnitude of the registered signal, indicating that the HS chains were somehow involved in the unfolding process or in destabilizing the core protein, resulting in more complete denaturation for the Gpc-1 ΔGPI PG [Figure 5A (◇)]. The far-UV CD spectrum of Gpc-1 ΔGPI PG was recorded at 20 °C, after it had been heated to 90 °C and cooled from 90 to 20 °C (Figure 5B). Most of the molar ellipticity was lost when Gpc-1 ΔGPI PG was heated to 90 °C. When it was cooled to 20 °C, 96% of the signal was regained for the peak at 195 nm, but only 73% for the trough at 208 nm, indicating that refolding of Gpc-1 ΔGPI PG after heat denaturation was not completely reversible.

To investigate the heat denaturation of rhGpc-1 in greater depth, we performed DSC experiments. His_6-Gpc-1 ΔGPI PG at a concentration of 0.5 mg/mL was heated at a rate of 1 °C/min from 10 to 90 °C. The DSC profile showed a single peak with a maximum at ~68 °C [Figure 6A (—)]. Cooling and rescanning of the sample showed that the thermal unfolding of His_6-Gpc-1 PG is at least partly reversible [Figure 6A (– – –)], thus confirming the result obtained by CD spectroscopy (Figure 5A,B). The DSC profiles of the His_6-Gpc-1 ΔGPI core protein and His_6-Gpc-1 ΔGPI ΔHS (also at a concentration of 0.5 mg/mL) were similar to the PG DSC profile, but unfolding occurred at a slightly higher temperature, ~71 °C [Figure 6B,C (—)], and no or very little refolding was detected for these proteins [Figure 6B,C (– – –)]. To further investigate the role of HS in refolding after heat denaturation, we performed DSC experiments with the three forms of His_6-Gpc-1 at two concentrations, 0.1 and 1 mg/mL. For the concentrations used, 60% refolding was observed for His_6-Gpc-1 ΔGPI PG. For the two different rhGpc-1 core protein forms, 40% refolding was seen at a protein concentration of 0.1 mg/mL whereas very little refolding was seen at 0.5 and 1 mg/mL (Table 1). This indicates that refolding was concentration-dependent for recombinant His_6-Gpc-1 devoid of O-linked glycosylation, but concentration-independent for the His_6-Gpc-1 PG form.

Although thermal unfolding was not completely reversible, we tried to deconvolute the experimental data. This can be done if

the irreversible step takes place at a higher temperature than the calorimetric transition (*30*). Almost complete refolding, ~90%, was seen when rhGpc-1 PG was heated to 80 °C (data not shown), indicating that the irreversible step takes place after the calorimetric transition. The DSC profile of His_6-Gpc-1 ΔGPI PG at ~0.1 mg/mL was fitted using a non-two-state model (eqs 12 and 13) to calculate the calorimetric heat change (ΔH) and van't Hoff heat change (ΔH_v). The ratio between ΔH and ΔH_v can be used to evaluate the mode of unfolding. The theoretical $\Delta H/\Delta H_v$ value for a dimeric protein unfolding in a single coupled transition is 0.5; the theoretical value for a single-domain protein that unfolds without intermediates is 1, and the theoretical value for a protein consisting of two identical domains that unfold independently at the same midpoint temperature (T_m) is 2 (*31*). The $\Delta H/\Delta H_v$ ratio for His_6-Gpc-1 ΔGPI PG at ~0.1 mg/mL was 1.01 (Table 2), suggesting that the unfolding transition proceeds from native to unfolded without any intermediates in a two-state process. We therefore used a two-state model of unfolding (eq 10 and 11) to fit the experimental data. The experimental data (solid line), the fitted curve for the non-two-state model (dashed line), and the fitted curve for the two-state model (dotted line) are shown in Figure 7A. The fitted curves for the non-two-state and two-state models overlap, which also suggests that unfolding follows a two-state mechanism. Thus, the two-state model was used to calculate T_m and ΔH (Table 2). The heat capacity change at T_m (ΔC_p) was determined by extrapolation of the pre- and post-transition baselines, and the Gibbs free energy at 20 °C, $\Delta G(20)$, was calculated to be 55 kJ/mol using eq 14. The $\Delta G(20)$ value of 55 kJ/mol is in good agreement with the values obtained from the analysis of the urea and guandine-HCl denaturation curves. However, this value should be interpreted with caution because of difficulties in determining ΔC_p for a reaction that is not completely reversible. Fitting of His_6-Gpc-1 ΔGPI core protein and His_6-Gpc-1 ΔGPI ΔHS at a concentration of 0.1 mg/mL using a non-two-state model yielded a $\Delta H/\Delta H_v$ ratio of ~0.8 (Table 2), suggesting that unfolding of the core protein does not follow a two-state model. The fitted curves for the non-two-state (– – –) and two-state (···) models for His_6-Gpc-1 ΔGPI core protein and His_6-Gpc-1 ΔGPI ΔHS are shown in panels B and C of Figure 7. Here, the best fit was obtained using the non-two-state model. Calorimetric data for the three different forms of recombinant Gpc-1 at ~0.1 and ~0.5 mg/mL are listed in Table 2. $\Delta G(20)$ values were not calculated for the two different core protein forms, since unfolding did not follow a two-state mechanism and because of difficulties in determining ΔC_p. Taken together, the heat denaturation results suggest that O-glycosylation protects the Gpc-1 core protein from irreversible aggregation.

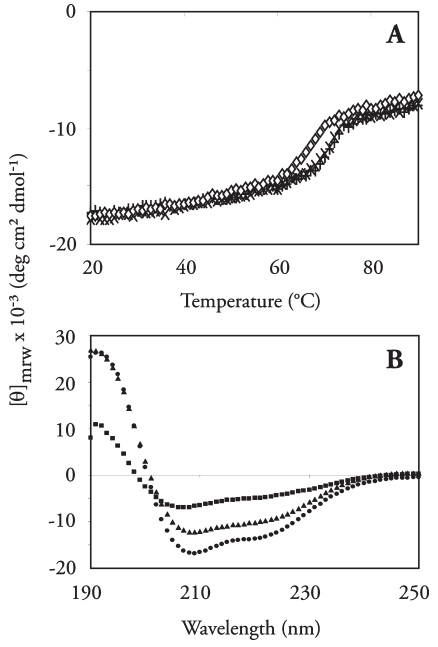

FIGURE 5: Heat denaturation of rhGpc-1 monitored by far-UV CD. (A) Heat denaturation of Gpc-1 ΔGPI PG (◇), Gpc-1 ΔGPI core protein (×), and Gpc-1 ΔGPI ΔHS (+) was monitored by ellipticity at 208 nm. The heating rate was 1 °C/h. (B) Far-UV CD spectra of Gpc-1 ΔGPI PG in 20 mM sodium phosphate (pH 7.4) at 20 °C (○), at 90 °C (□), or cooled to 20 °C (△).

Table 1: T_m and Refolding of rhGpc-1 at Different Concentrations[a]

	~0.1 mg/mL	~0.5 mg/mL	~1.0 mg/mL
His_6-Gpc-1 ΔGPI PG			
apparent T_m (°C)	67.6	67.7	67.9
refolding (%)	63	61	62
His_6-Gpc-1 ΔGPI core protein			
apparent T_m (°C)	71.0	71.2	71.2
refolding (%)	42	2	3
His_6-Gpc-1 ΔGPI ΔHS			
apparent T_m (°C)	70.4	71.3	71.5
refolding (%)	41	5	2

[a]Samples of rhGpc-1 were scanned in the microcalorimeter as described in the legend of Figure 6. The apparent T_m is given as the temperature at maximum heat capacity for the endotherm. Refolding was calculated by comparing the area of the endotherm for the first and second scans after subtraction of the baseline.

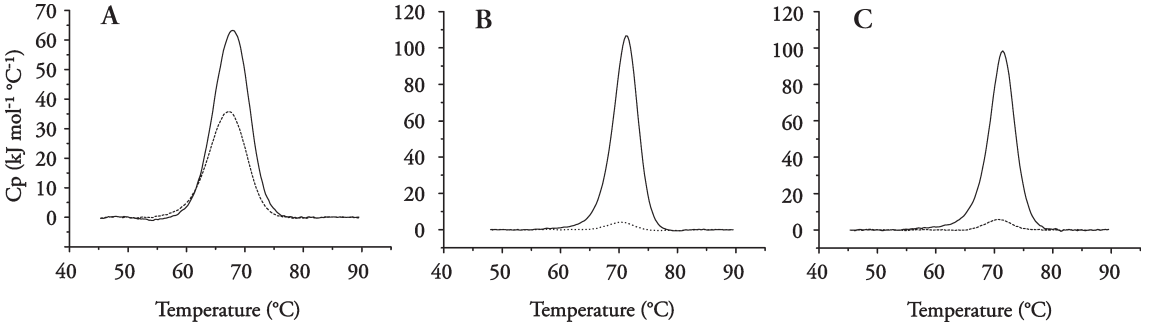

FIGURE 6: Heat denaturation of rhGpc-1 studied by DSC. DSC profiles of (A) His_6-Gpc-1 ΔGPI PG, (B) His_6-Gpc-1 ΔGPI core protein, and (C) His_6-Gpc-1 ΔGPI ΔHS at a concentration of 0.5 mg/mL. Samples were scanned from 10 to 90 °C. The heating rate was 1 °C/h: (—) first heating scan and (– – –) second heating scan. Buffer−buffer scan reference data were subtracted from all calorimetric traces.

Table 2: Thermodynamic Parameters for the Different Forms of rhGpc-1 at Different Concentrations (N2S, non-two-state; 2S, two-state)

protein	concn (mg/mL)	T_m (N2S) (°C)	ΔH (N2S) (kJ/mol)	ΔH_v (N2S) (kJ/mol)	ΔH (N2S)/ ΔH_v (N2S)	T_m (2S) (°C)	ΔH (2S) (kJ/mol)	ΔC_p (kJ mol^{-1} °C^{-1})	ΔG(20) (kJ/mol)
His_6-Gpc-1 ΔGPI PG	0.16	67.4	494	491	1.01	67.4	492	3.86	55.2
His_6-Gpc-1 ΔGPI PG	0.52	67.7	494	512	0.96	67.7	502	3.78	57.0
His_6-Gpc-1 ΔGPI core protein	0.13	71.0	501	595	0.84	na	na	na	na
His_6-Gpc-1 ΔGPI core protein	0.67	71.1	583	720	0.81	na	na	na	na
His_6-Gpc-1 ΔGPI ΔHS	0.15	70.0	444	563	0.79	na	na	na	na
His_6-Gpc-1 ΔGPI ΔHS	0.55	71.3	563	682	0.83	na	na	na	na

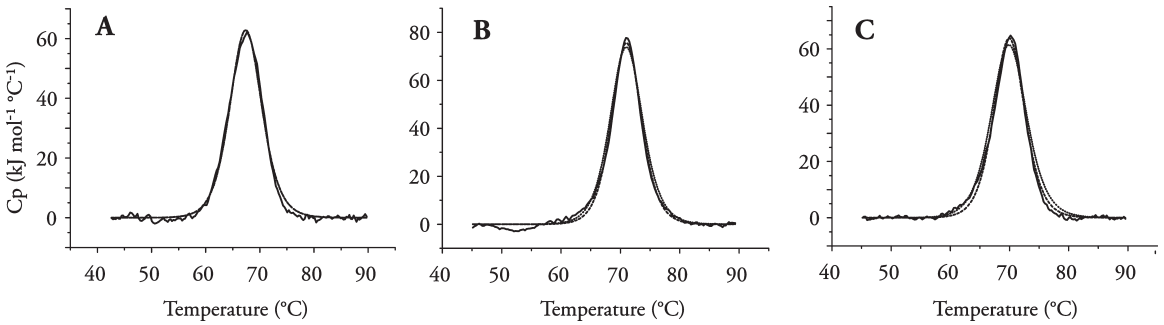

FIGURE 7: Curve fitting of rhGpc-1 DSC profiles. DSC profiles of (A) His_6-Gpc-1 ΔGPI PG, (B) His_6-Gpc-1 ΔGPI core protein, and (C) His_6-Gpc-1 ΔGPI ΔHS at a concentration of 0.1 mg/mL. Buffer−buffer scan reference data were subtracted from all calorimetric traces: (—) experimental data and (− − −) fitted curves using a non-two-state model and (· · ·) fitted curves using a two-state model. The dashed and dotted lines overlap in panel A.

DISCUSSION

In a previous study, we investigated the biological activity of secreted rhGpc-1 with respect to S-nitrosylation and demonstrated that the secreted nonglycanated rhGpc-1 core protein contains free Cys residues that can become S-nitrosylated by NO donor and $CuCl_2$ (*17*). Addition of ascorbate to rhGpc-1 PG resulted in NO-dependent autocleavage of the HS side chains at N-unsubstituted glucosamines. Furthermore, the rhGpc-1 produced in the presence of polyamine synthesis inhibitor, α-difluoromethylornithine, became endogenously S-nitrosylated, and the content of N-unsubstituted glucosamine residues in the HS chains increased (*17*). In this investigation, Gpc-1 ΔGPI and Gpc-1 ΔGPI ΔHS were expressed in human embryonic kidney cells. Gpc-1 ΔGPI was secreted both as PG and as core protein, and Gpc-1 ΔGPI ΔHS was secreted solely as core protein. The three different forms of secreted rhGpc-1 were purified and investigated using CD, fluorescence, and DSC to study the conformation and stability of Gpc-1 core protein. We have shown here that Gpc-1 has a stable core protein as high concentrations of urea or guandine-HCl (5.8 or 2.6 M, respectively), or high temperatures (~70 °C) were required to denature the protein. Stability studies of other PGs, decorin and biglycan, demonstrate lower stability with a T_m around 45−46 °C and denaturation at 0.75 and 0.95 M guandine-HCl for decorin and biglycan, respectively (*24*). Unfolding of the rhGpc-1 core protein in urea or guanidine-HCl occurred in a single step for both secondary and tertiary structure, and unfolding data closely fitted a two-state model, indicating a highly cooperative unfolding process. Our estimate of $\Delta H_v/\Delta H$ for thermal unfolding of His_6-Gpc-1 ΔGPI PG monitored by DSC was very close to 1, also indicating a highly cooperative unfolding process. By deconvolution of the urea and guandine-HCl denaturation curves and of the DSC profile, ΔG_{N-U} of Gpc-1 was estimated to be ~60 kJ/mol. This value is in the higher range of what is usually seen for globular proteins, which have ΔG_{N-U} values between 20 and 60 kJ/mol (see ref *32* and references therein), indicating that Gpc-1 core protein is a densely packed globular protein. The Gpc-1 core protein contains 16 Cys residues that may be involved in protein stabilization. Preliminary results from the study of heat denaturation of rhGpc-1 in the presence of reducing agents point toward the destabilizing effect of such agents with a decrease in *T*m indicating the presence disulfide bonds. However, the factors involved in Gpc-1 stability and the functional implications remain to be investigated. Glypicans can be secreted from the cell surface and thereby act as competitive inhibitors of growth factor signaling (*11*, *33*). The stable Gpc-1 may allow the shedded PG to remain in the tissues for a long time, sequestering growth factors, which thereby become unavailable to the cells.

On the basis of primary structures and sequence homology between glypicans, the glypican core proteins have been thought to consist of a large N-terminal Cys-rich globular domain and a GAG attachment domain. The large globular domain has been shown to influence GAG class determination and preferential HS assembly (*34*). Deconvolution of the far-UV CD spectrum of rhGpc-1 showed that the Gpc-1 core protein is predominantly α-helical in structure, with the secondary fractions estimated to be 42% in α-helical structure, 13% in β-sheet conformation, 18% in turns, and 27% unordered. We can thus speculate that the α-helical and β-sheet conformations are part of a densely packed globular domain and that the turns and unordered structures are part of a GAG attachment domain. However, the steepness of the transition zone data in the denaturation curves and the close fit to a two-state model for the His_6-Gpc-1 ΔGPI PG DSC profile indicate a highly cooperative unfolding, which suggests that the Gpc-1 core protein is a single-domain protein. This is surprising, as the structure of a large protein (> 20 kDa) is often subdivided into several domains that unfold independently (*32*).

The far-UV CD spectra for the three forms of rhGpc-1 were identical (Figure 3), indicating that the variations cause no

change in secondary structure. Also, the fluorescence emission spectra were similar with identical emission maxima (Figure 4), indicating highly similar tertiary structure. Moreover, the PG form of rhGpc-1 was slightly less stable than the core protein form, as shown by heat denaturation monitored by CD and by DSC (Figures 5 and 6), suggesting that there is no stabilizing interaction between HS chains and the core protein in the native state (*35*). Recent reports using constructs that express glypicans without HS have suggested a distinct role for the core proteins in growth factor signaling. The core protein of the *Drosophila melanogaster* glypican Dally binds to BMP4 and can at least in part rescue *dally* mutant phenotypes (*10*). The glypican-3 core protein binds to the growth factor hedgehog and induces endocytosis and degradation of hedgehog (*9*). On the basis of the findings presented here, that the HS chains do not affect the structure or stabilize the native rhGpc-1 PG, it is reasonable to suggest that no perturbing interactions occur between the HS chains and the core protein. The exposed core protein, which is not blocked by the HS chains, can fulfill a role of its own, as seen in binding of BMP4 to the Dally core protein and of hedgehog to the glypican-3 core protein. We can therefore speculate that the functional role of mammalian glypican-1−6 core proteins lies in their ability to directly bind to different growth factors.

We have shown in this paper that very little refolding occurred for the rhGpc-1 core protein upon cooling and rescanning of a sample that had been unfolded by heating to 90 °C (Table 1). This result was obtained with sample concentrations of 0.5 and 1 mg/mL. However, 60% refolding was seen at the same concentrations with His_6-Gpc-1 ΔGPI PG, indicating that the HS chains protected the core protein from heat-induced irreversible denaturation. Some refolding occurred for the rhGpc-1 core protein at 0.1 mg/mL, suggesting that refolding in this form of Gpc-1 was dependent on concentration.

Exogenous GAGs have been used as additives to prevent protein aggregation, but the mechanism has not been elucidated in detail (*36*). There are three possible mechanisms that could explain why the HS chains attached to heat-denatured Gpc-1 can prevent aggregation. The first possible mechanism is one in which the HS chains bind to the native core protein and thereby stabilize the structure, which would facilitate refolding (*35*). This is most likely not the case, as the heat denaturation experiments showed that the PG form of Gpc-1 is less stable than the core protein form. The second possible mechanism is one in which the HS chains bind to the unfolded protein and thereby create a protein−HS complex with a highly negative net charge, which would increase the solubility and thereby facilitate refolding (*36*, *37*). The slightly reduced stability of the PG form of rhGpc-1 speaks in favor of this mechanism. In contrast to the situation where GAGs are added exogenously, the HS chains are covalently attached to the core protein in the Gpc-1 PG. Thus, we might speculate that additional charge from the HS chains renders the PG form of Gpc-1 more soluble than the core protein form. The third possible mechanism is one in which electrostatic repulsion between an acidic protein and the polyanionic GAGs would prevent aggregation (*38*). The rhGpc-1 used in this study has a pI of 6.2, and it is thus negatively charged under the conditions used. Reversibility of unfolding for Gpc-1 ΔGPI core protein was dependent on protein concentration, which suggests that intermolecular processes are involved in irreversible unfolding. On the other hand, reversibility of Gpc-1 ΔGPI PG was found to be independent of protein concentration, suggesting that the HS chains prevent intermolecular interactions. Moreover, deconvolution of the DSC data for the PG form indicated that the heat denaturation followed a two-state mechanism (Table 2 and Figure 7A), suggesting that Gpc-1 ΔGPI PG is in a monomeric state. Deconvolution of the DSC data for Gpc-1 ΔGPI core protein and Gpc-1 ΔGPI ΔHS proved to be more complex and fitted best to a non-two-state model, suggesting that intermediate states were present during the unfolding or that the core protein was in a multimeric state. The increased stability of rhGpc-1 core protein over PG as seen in the heat denaturation experiments could be due to protein−protein interactions in the native state when the HS chains are not present. The results described in this study thus invite inquiries into the possibility that the HS chains on Gpc-1 prevent aggregation, probably by providing additional negative charge to the core protein and from electrostatic repulsion between the acidic core protein and the polyanionic HS chains. However, it is important to mention that the very important function of glypicans in growth factor signaling has mainly been related to their HS chains.

ACKNOWLEDGMENT

We thank Prof. Lars-Åke Fransson (Lund University) for support, Sebastian Kalamajski (Lund University) for help with the CD and DSC experiments, and Patrik Önnerfjord (Lund University) for help with the MALDI-TOF experiment.

REFERENCES

1. Bülow, H. E., and Hobert, O. (2006) The Molecular Diversity of Glycosaminoglycans Shapes Animal Development. *Annu. Rev. Cell Dev. Biol. 22*, 375–407.
2. Belting, M. (2003) Heparan sulfate proteoglycan as a plasma membrane carrier. *Trends Biochem. Sci. 28*, 145–151.
3. Fransson, L. Å., Belting, M., Cheng, F., Jönsson, M., Mani, K., and Sandgren, S. (2004) Novel aspects of glypican glycobiology. *Cell. Mol. Life Sci. 61*, 1016–1024.
4. David, G., Lories, V., Decock, B., Marynen, P., Cassiman, J. J., and Van den Berghe, H. (1990) Molecular cloning of a phosphatidylinositol-anchored membrane heparan sulfate proteoglycan from human lung fibroblasts. *J. Cell Biol. 111*, 3165–3176.
5. Bernfield, M., Gotte, M., Park, P. W., Reizes, O., Fitzgerald, M. L., Lincecum, J., and Zako, M. (1999) Functions of cell surface heparan sulfate proteoglycans. *Annu. Rev. Biochem. 68*, 729–777.
6. Topczewski, J., Sepich, D. S., Myers, D. C., Walker, C., Amores, A., Lele, Z., Hammerschmidt, M., Postlethwait, J., and Solnica-Krezel, L. (2001) The zebrafish glypican knypek controls cell polarity during gastrulation movements of convergent extension. *Dev. Cell 2*, 251–264.
7. Veugelers, M., Cat, B. D., Muyldermans, S. Y., Reekmans, G., Delande, N., Frints, S., Legius, E., Fryns, J.-P., Schrander-Stumpel, C., Weidle, B., Magdalena, N., and David, G. (2000) Mutational analysis of the GPC3/GPC4 glypican gene cluster on Xq26 in patients with Simpson-Golabi-Behmel syndrome: Identification of loss-of-function mutations in the GPC3 gene. *Hum. Mol. Genet. 9*, 1321–1328.
8. Yan, D., and Lin, X. (2008) Opposing roles for glypicans in Hedgehog signalling. *Nat. Cell Biol. 10*, 761–763.
9. Capurro, M. I., Xu, P., Shi, W., Li, F., Jia, A., and Filmus, J. (2008) Glypican-3 inhibits Hedgehog signaling during development by competing with patched for Hedgehog binding. *Dev. Cell 14*, 700–711.
10. Kirkpatrick, C. A., Knox, S. M., Staatz, W. D., Fox, B., Lercher, D. M., and Selleck, S. B. (2006) The function of a *Drosophila* glypican does not depend entirely on heparan sulfate modification. *Dev. Biol. 300*, 570–582.
11. Capurro, M. I., Xiang, Y.-Y., Lobe, C., and Filmus, J. (2005) Glypican-3 promotes the growth of hepatocellular carcinoma by stimulating canonical Wnt signaling. *Cancer Res. 65*, 6245–6254.
12. Herndon, M. E., Stipp, C. S., and Lander, A. D. (1999) Interactions of neural glycosaminoglycans and proteoglycans with protein ligands: Assessment of selectivity, heterogeneity and the participation of core proteins in binding. *Glycobiology 9*, 143–155.

13. Rapraeger, A. C., and Ott, V. L. (1998) Molecular interactions of the syndecan core proteins. *Curr. Opin. Cell Biol. 10*, 620–628.
14. Bass, M. D., and Humphries, M. J. (2002) Cytoplasmic interactions of syndecan-4 orchestrate adhesion receptor and growth factor receptor signalling. *Biochem. J. 368*, 1–15.
15. Lim, S. T., Longley, R. L., Couchman, J. R., and Woods, A. (2003) Direct binding of syndecan-4 cytoplasmic domain to the catalytic domain of protein kinase Cα (PKCα) increases focal adhesion localization of PKCα. *J. Biol. Chem. 278*, 13795–13802.
16. Ding, K., Mani, K., Cheng, F., Belting, M., and Fransson, L. Å. (2002) Copper-dependent autocleavage of glypican-1 heparan sulfate by nitric oxide derived from intrinsic nitrosothiols. *J. Biol. Chem. 277*, 33353–33360.
17. Svensson, G., and Mani, K. (2009) S-Nitrosylation of secreted recombinanat human glypican-1. *Glycoconjugate J.,* in press (doi:10.1007/s10719-009-9243-z).
18. Mani, K., Cheng, F., Havsmark, B., Jönsson, M., Belting, M., and Fransson, L. Å. (2003) Prion, amyloid *β*-derived Cu(II) ions, or free Zn(II) ions support S-nitroso-dependent autocleavage of glypican-1 heparan sulfate. *J. Biol. Chem. 278*, 38956–38965.
19. Cappai, R., Cheng, F., Ciccotosto, G. D., Needham, B. E., Masters, C. L., Multhaup, G., Fransson, L. Å., and Mani, K. (2005) The amyloid precursor protein (APP) of Alzheimer disease and its paralog, APLP2, modulate the Cu/Zn-nitric oxide-catalyzed degradation of glypican-1 heparan sulfate in vivo. *J. Biol. Chem. 280*, 13913–13920.
20. Mani, K., Jönsson, M., Edgren, G., Belting, M., and Fransson, L. Å. (2000) A novel role for nitric oxide in the endogenous degradation of heparan sulfate during recycling of glypican-1 in vascular endothelial cells. *Glycobiology 10*, 577–586.
21. Cheng, F., Mani, K., van den Born, J., Ding, K., Belting, M., and Fransson, L. Å. (2002) Nitric oxide-dependent processing of heparan sulfate in recycling S-nitrosylated glypican-1 takes place in caveolin-1-containing endosomes. *J. Biol. Chem. 277*, 44431–44439.
22. Mani, K., Cheng, F., and Fransson, L. Å. (2006) Defective nitric oxide-dependent, deaminative cleavage of glypican-1 heparan sulfate in Niemann-Pick C1 fibroblasts. *Glycobiology 16*, 711–718.
23. Scott, P. G., McEwan, P. A., Dodd, C. M., Bergmann, E. M., Bishop, P. N., and Bella, J. (2004) Crystal structure of the dimeric protein core of decorin, the archetypal small leucine-rich repeat proteoglycan. *Proc. Natl. Acad. Sci. U.S.A. 101*, 15633–15638.
24. Scott, P. G., Dodd, C. M., Bergmann, E. M., Sheehan, J. K., and Bishop, P. N. (2006) Crystal structure of the biglycan dimer and evidence that dimerization is essential for folding and stability of class I small leucine-rich repeat proteoglycans. *J. Biol. Chem. 281*, 13324–13332.
25. Bengtsson, E., Aspberg, A., Heinegard, D., Sommarin, Y., and Spillmann, D. (2000) The Amino-terminal Part of PRELP Binds to Heparin and Heparan Sulfate. *J. Biol. Chem. 275*, 40695–40702.
26. Sreerama, N., and Woody, R. W. (2000) Estimation of Protein Secondary Structure from Circular Dichroism Spectra: Comparison of CONTIN, SELCON, and CDSSTR Methods with an Expanded Reference Set. *Anal. Biochem. 287*, 252–260.
27. Santoro, M. M., and Bolen, D. W. (1988) Unfolding free energy changes determined by the linear extrapolation method. 1. Unfolding of phenylmethanesulfonyl α-chymotrypsin using different denaturants. *Biochemistry 27*, 8063–8068.
28. Pace, C. N., and Shaw, K. L. (2000) Linear extrapolation method of analyzing solvent denaturation curves. *Proteins: Struct., Funct., Genet. 41*, 1–7.
29. Ramamurthy, P., Hocking, A. M., and McQuillan, D. J. (1996) Recombinant decorin glycoforms. Purification and structure. *J. Biol. Chem. 271*, 19578–19584.
30. Sanchez-Ruiz, J. M. (1992) Theoretical analysis of Lumry-Eyring models in differential scanning calorimetry. *Biophys. J. 61*, 921–935.
31. Makhatadze, G. (1998) Measuring Protein Thermostability by Differential Scanning Calorimetry. In Current Protocols in Protein Science , John Wiley & Sons, New York.
32. Makhatadze, G. I., and Privalov, P. L. (1995) Energetics of Protein Structure. In Advances in Protein Chemistry , Academic Press, San Diego.
33. Traister, A., Shi, W., and Filmus, J. (2008) Mammalian Notum induces the release of glypicans and other GPI-anchored proteins from the cell surface. *Biochem. J. 410*, 503–511.
34. Chen, R. L., and Lander, A. D. (2001) Mechanisms underlying preferential assembly of heparan sulfate on glypican-1. *J. Biol. Chem. 276*, 7507–7517.
35. Waldron, T. T., and Murphy, K. P. (2003) Stabilization of proteins by ligand binding: Application to drug screening and determination of unfolding energetics. *Biochemistry 42*, 5058–5064.
36. Chung, K., Kim, J., Cho, B.-K., Ko, B.-J., Hwang, B.-Y., and Kim, B.-G. (2007) How does dextran sulfate prevent heat induced aggregation of protein?: The mechanism and its limitation as aggregation inhibitor. *Biochim. Biophys. Acta 1774*, 249–257.
37. Lawrence, M. S., Phillips, K. J., and Liu, D. R. (2007) Supercharging proteins can impart unusual resilience. *J. Am. Chem. Soc. 129*, 10110–10112.
38. Tsai, A. M., van Zanten, J. H., and Betenbaugh, M. J. (1998) Electrostatic effect in the aggregation of heat-denatured RNase A and implications for protein additive design. *Biotechnol. Bioeng. 59*, 281–285.